Dalton Transactions

Cite this: *Dalton Trans.*, 2011, **40**, 146

www.rsc.org/dalton

PAPER

Unsymmetrical diimine complexes of iron(II) and manganese(II): synthesis, structure and photoluminescence of an isomer†

Amit Saha Roy,[a] Manas Kumar Biswas,[a] Thomas Weyhermüller[b] and Prasanta Ghosh*[a]

Received 21st July 2010, Accepted 27th September 2010
DOI: 10.1039/c0dt00883d

Two bis(unsymmetrical diimine) complexes of $(L_{NO_2}{}^{\phi 1})(L_{NO_2}{}^{\phi 2})M^{II}Cl_2$ family with M = Fe and Mn, are reported ($L_{NO_2}{}^{\phi}$ = (*E*)-3-nitro-*N*-(pyridine-2-ylmethylene)aniline; ϕ = dihedral angle between the diimine unit including pyridine ring and the phenyl ring planes). Pure *tcc*-$(L_{NO2}{}^{33.6})(L_{NO2}{}^{79.3})Fe^{II}Cl_2 \cdot 0.5H_2O$ (**1**) and *tcc*-$(L_{NO2}{}^{32.0})(L_{NO2}{}^{79.4})Mn^{II}Cl_2 \cdot 0.5H_2O$ (**2**) isomers have been successfully isolated in high yields and characterized by elemental analyses, variable temperature magnetic susceptibility measurements, IR, mass, UV-vis and Mössbauer spectra including the single-crystal X-ray structure determinations that identified strong intermolecular non-bonding interactions in lattice (*tcc* refers to *trans–cis–cis* positions with respect to pyridine N-imine N–Cl donors). Geometries optimizations of all possible *tcc*, *ttt*, *ctc*, *ccc* and *cct* isomers of iron at the B3LYP/DFT level in gas-phase have shown that the *tcc*-isomer incorporating two non-equivalent ligands as in $(L_{NO_2}{}^{42})(L_{NO_2}{}^{61})Fe^{II}Cl_2$, **1** (g), is stabilized by 6–20 kJ mol^{-1} compared to other isomers where two ligands are equivalent. The frozen methanol glasses of **1** and **2** are luminescent at 77 K (**1**: λ_{ext} = 370, λ_{em} = 521 nm, χ^2 = 1.3, τ_{avg} = 0.57 ns; **2**: λ_{ext} = 368, λ_{em} = 524 nm, χ^2 = 1.1, τ_{avg} = 0.90 ns). The DFT calculations have identified four closely spaced localized π^* orbitals comprising of two non-equivalent ligands as UPMOs. The features contrast the *tcc*-isomer of $(L^{\phi})_2Fe^{II}Cl_2$ (**3**), congener of **1** without $-NO_2$ substitution and non-emissive $(bpy)_2Fe^{II}Cl_2$ (**4**) where two ligands are equivalent. TD-DFT calculations have assigned intra-ligand (IL) and ligand to ligand charge transfer (LLCT) dominated excited states as the origin of luminescence of **1** and **2**.

Introduction

Localization of the electronically excited charge that causes a net dipole moment change with respect to the ground state of a chromophore is a herald of encoding photo energy at the molecular level. This important factor is mainly controlled by the structure of the unoccupied photoactive molecular orbitals (UPMOs) of the species. Evidently, the modification of the UPMOs is one of the important steps to tune the photoactivity. Chemically it can be achieved by changing the substitution on the chromophore. For this study, transition metal (source of electron) bound conjugated fragment (electron sink) is one of the basic units. In this unit, UPMOs are mainly centered on conjugated diimine fragment and behave like sinks for excited state. Enormous possibility of the activity can be developed to such molecular unit by tuning the UPMOs. Components of the UPMOs affect the excited charge delocalization. Metal bound α-diimine chromophore is photoactive due to MLCT and in some cases due to the $\pi_{diimine}$ to $\pi_{diimine}{}^*$ charge transfer.[1–13]

An assortment of the photophysical properties of such molecule is possible by tuning the conjugation of the photoactive π* orbital of the α-diimine core and substitution. Two most strong and rigid chelating heterocyclic symmetrical α-diimines are 2,2′-bipyridine (bpy) and 1,10-phenanthroline (phen) which form easily tris(diimine), $ML_3{}^{3+}$ type of species (L = bpy, phen) with transition metal ions. The ruthenium *tris*-diimine adduct, $Ru(bpy)_3{}^{3+}$ with its ^{3}MLCT excited state[14] is strongly emissive and now is a commonly used chromophore to build new luminophores with two and three component systems, *i.e.*, dyads and triads, to investigate photoinduced charge separation (CS).[15] The iron congener of it, *i.e.*, $Fe(bpy)_3{}^{3+}$ is non-emissive because of its low-lying ^{3}(d–d) state.[16] *cis*-Dihalobis(diimine)M(II) complexes of these diimines as $M(bpy)_2Cl_2$ and $M(phen)_2Cl_2$ are potential precursors[17] but hard to achieve with 3d metal ions.[18] They are high spin and non-emissive.[19]

Modification of the diimine π^* orbital to achieve a more localized or delocalized excited state with higher excitation probabilities and to change the transition energy is momentous for photoactivity. The energy of the $\pi_{diimine}{}^*$ orbital of course is a function of the conjugation with the substituent on N atoms. It is hard to perturb the chromophore **I** (Chart 1). But the chromophore **II** incorporates an unsymmetrical diimine ($L_H{}^{\phi}$) and

[a]*Department of Chemistry, R. K. Mission Residential College, Narendrapur, Kolkata-103, India. E-mail: ghoshp_chem@yahoo.co.in; Fax: +91-33-2477-3597; Tel: +91-33-2428-7017*
[b]*Max-Planck-Institut für Bioanorganische Chemie, Stiftstrasse 34-36, D-45470, Mülheim an der Ruhr, Germany*

† CCDC reference numbers 668788 and 770797 respectively for **1** and **2**. For crystallographic data in CIF or other electronic format see DOI: 10.1039/c0dt00883d

the energies of both the $\pi_{diimine}^*$ and $\pi_{diimine}$ orbitals depend on the ϕ (ϕ = dihedral angle between the diimine unit including the pyridine ring and phenyl ring planes). In **II** and **III**, rotation of phenyl rings around =N–C single bond as shown in Chart 1 inhibits the conjugation and the rotation of phenyl rings makes the ligands non-equivalent.

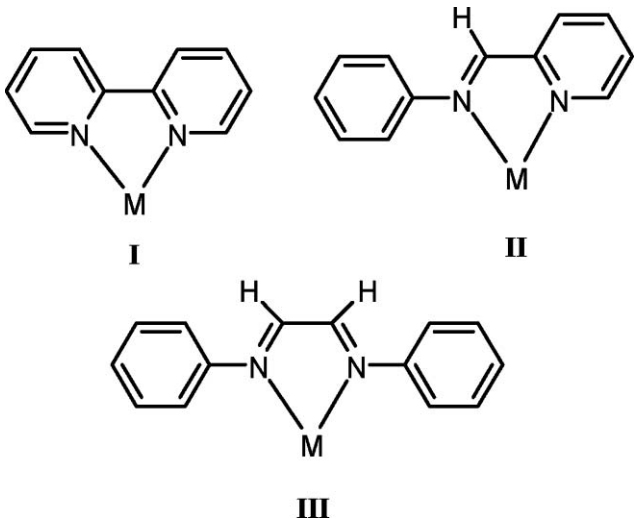

Chart 1 (bpy)M (**I**), (L_H^{ϕ})M (**II**) and ($L_H^{\phi 1\phi 2}$)M (**III**) chromophores.

Calculations at the B3LYP level of DFT on the free L_H^{ϕ} ligand of **II** in gas phase using 6-31G basis set for all atoms have shown that the energies of both the HOMO ($\pi_{diimine}$) and LUMO ($\pi_{diimine}^*$) depend on the dihedral angle (ϕ). Both the HOMO and LUMO have the minimum energy at the dihedral angle $\phi = 0$ or 180° and both have the maximum energy at $\phi = 90°$ where the conjugation is less as shown in Chart 2(a). At $\phi = 90°$, the contribution of the phenyl ring to the LUMO is the minimum. Again, the calculations show that the difference of energy of HOMO and LUMO is also minimum at $\phi = 90$ (Chart 2(b)). Thus, rotation in conjunction with the solvation can have an immense impact on the photophysical properties of such coordinated diimine systems and is a subject of research here. In the metal bound diimine species, the absorption and emission features are primarily controlled by the energy of the unoccupied π^* orbital and its spatial localization. Particularly, for bis- or tris(diimine)M species, the orientations are important as two or more diimines with different dihedral angle (ϕ) will act as an independent chromophore. They will create a cluster of closely-spaced UPMO. To follow in a metal complex, it demands experimental verification.

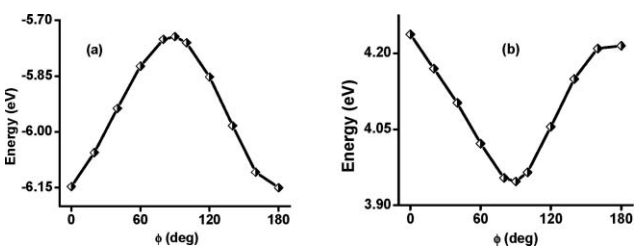

Chart 2 (a) Change of the energy of HOMO (E_{HOMO}) and (b) $E_{LUMO} - E_{HOMO}$ (eV) with respect to ϕ in L_H^{ϕ} (gas phase).

The α-diimine ligand ($L_{NO_2}^{\phi}$) that has been used in this work, is (*E*)-3-nitro-*N*-(pyridine-2-ylmethylene)aniline. Recently, Scott *et al.* reported the optically active *fac*-tris(diimine)Fe(II) complexes with this type of NN donor ligands.[20] In this work, we have been successful in isolating only *tcc*-isomers of the $(L_{NO_2}^{\phi 1})(L_{NO_2}^{\phi 2})M^{II}Cl_2$ family as products where the two ligands are non-equivalent in the crystal lattice (since this is shown by XRD), and are likewise calculated to be non-equivalent in the gas phase, since this cannot be measured directly (dihedral angles $\phi 1$ and $\phi 2$ correspond to two diimine ligands; *tcc* refers to *trans–cis–cis* positions with respect to pyridine N-imine N–Cl donors as shown in Fig. 1 and 2). The isomers in frozen methanol glasses are emissive at 77 K. This finding contrasts the $(bpy)_2MCl_2$ or $(phen)_2MCl_2$ species which are non-emissive. The molecular stereochemistry and the purity of the isolated isomer have been established by Mössbauer spectrum of **1** at 80 K, single-crystal X-ray structure determinations of **1** and **2** at 100 K and lifetime measurements of both in frozen methanol glasses at 77 K. Optimizations of geometries of all possible isomers at the B3LYP/DFT level in gas phase have shown that the two diimine ligands in all isomers are equivalent except in *tcc*-isomer which has the minimum ground state energy. Density functional

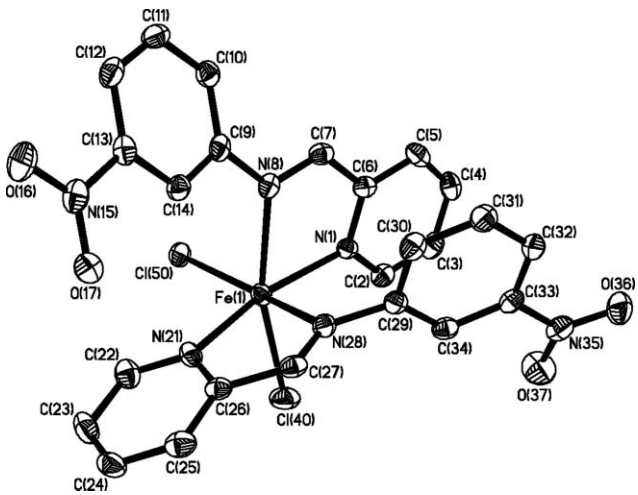

Fig. 1 Single-crystal X-ray structure of **1** (50% thermal ellipsoids). The water molecule and hydrogen atoms have been omitted for clarity.

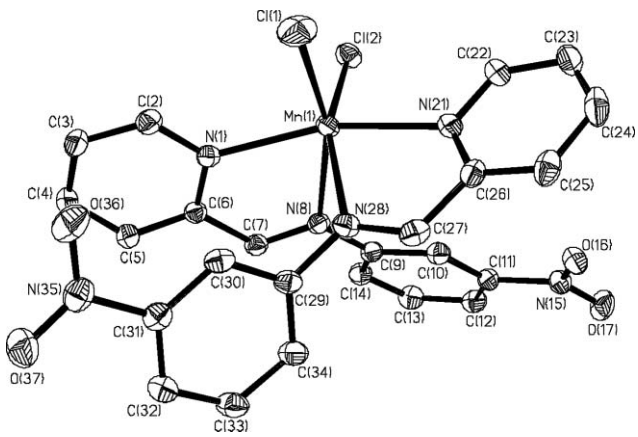

Fig. 2 Single-crystal X-ray structure of **2** (50% thermal ellipsoids). The water molecule and hydrogen atoms have been omitted for clarity.

theory (DFT) calculations have elucidated the structure of the occupied photoactive molecular orbitals (OPMOs) as well as the UPMOs and calibrated the effect of non-equivalnce of the two diimine ligands. Time-dependent density functional theory (TD DFT) calculations have assigned the emissive excited states and transition types of these luminescent members.

Experimental

Material and physical measurements

Reagents or analytical grade materials were obtained from commercial suppliers and used without further purification. Spectroscopic grade solvents were used for spectroscopic measurements. The C, H, N contents of the compounds were obtained from Perkin Elmer 2400 series II elemental analyzer. Infrared spectra of the samples were measured from 4000 to 400 cm^{-1} as KBr pellets at room temperature on a Perkin Elmer FT-IR-Spectrophotometer Spectrum RX 1. The temperature-dependent magnetic susceptibilities of the solid samples have been measured by using SQUID magnetometer. Zero-field Mössbauer spectrum of the polycrystalline bulk sample of **1** has been recorded at 80 K. Electronic absorption spectra in solution at 298 K were measured on a Perkin Elmer Lambda 25 spectrophotometer in the range 200–1100 nm. Emission spectra at 77 K were recorded in MeOH glass by using quartz sample tube on Perkin Elmer LS 55 luminescence spectrophotometer equipped with a Perkin–Elmer low-temperature luminescence accessory.

Syntheses

***tcc*-($L_{NO_2}^{33.6}$)($L_{NO_2}^{79.3}$)$Fe^{II}Cl_2$·0.5H_2O (1).** To 3-nitroaniline (280 mg, 2 mmol), 2-pyridinecarbaldehyde (330 mg, 3 mmol) was added and mixed well to form a paste. To this paste, methanol (25 mL) was added and heated at 50 °C and stirred for 15 min. The reaction mixture was cooled at 20 °C. To this solution mixture, $FeCl_2$, $4H_2O$ (200 mg, 1 mmol) and CH_2Cl_2 (5 mL) were added successively and stirred for 20 min. The solution was filtered. The dark green filtrate was collected and allowed to evaporate slowly in air. Within two days green crystals of **1** separated out, which were filtered and dried in air (single-crystals for X-ray structure were picked out from this product). Yield: 360 mg, 60% with respect to iron. ESI MS (CH_2Cl_2): m/z, 545.00 {**1**-(0.5H_2O + Cl)}$^+$. Elemental anal. (%) for $C_{24}H_{19}Cl_2FeN_6O_{4.5}$: calcd. C 48.84, H 3.24, N 14.23; Found: C 49.02, H 3.10, N 14.16; IR (KBr) (ν_{max}/cm^{-1}: 3430 (m), 1630 (m), 1593 (s), 1529 (vs), 1352 (vs), 1203 (m), 820 (s), 782 (s), 739 (s), 680 (m).

***tcc*-($L_{NO_2}^{32.0}$)($L_{NO_2}^{79.4}$)$Mn^{II}Cl_2$·0.5H_2O (2).** Orange crystals of **2** were prepared by the same procedure as above using $MnCl_2$, $4H_2O$. Yield: 350 mg, 60% with respect to manganese. ESI MS (CH_2Cl_2); m/z, 545.00 {**2**-(0.5H_2O + Cl)}$^+$. Elemental anal. (%) for $C_{24}H_{19}Cl_2MnN_6O_{4.5}$: calcd. C 48.92, H, 3.25, N 14.25; Found: C 49.12, H 3.20, N 14.10; IR (KBr) (ν_{max}/cm^{-1}: 3399 (m), 1630 (m), 1593 (s), 1529 (vs), 1352 (vs), 1201 (m), 1011 (s), 820 (s), 782 (s), 738 (s), 678 (m).

(*E*)-4-hydroxy-*N*-(pyridine-2-ylmethylene)aniline (L_{OH}). To 4-hydroxyaniline (215 mg, 2 mmol), 2-pyridinecarbaldehyde (214 mg, 2 mmol) was added and mixed well to form a paste. To this paste methanol (25 mL) was poured and heated to reflux for 15 min. Immediately a yellow solid separated out. The reaction mixture was cooled at 20 °C, filtered and the residue was dried in air. Yield: 285 mg (73% with respect to 4-hydroxyaniline). ESI MS (MeOH): m/z, 198.93; δ_H (300 MHz; DMSO-d_6; Me_4Si) 9.68 (s, O–H), 8.68 (1 H, d, 6-H), 8.60 (1 H, s, –N=CH), 8.12 (1 H, d, 3-H), 7.92 (1 H, t, 4-H), 7.48 (1 H, t, 5-H), 7.30 (2 H, d, 10-H & 14-H) and 6.83 (2 H, d, 11-H & 13-H). Elemental anal. (%) for $C_{12}H_{10}N_2O$: calcd. C 72.72, H 5.08, N 14.13. Found: C 72.69, H 5.01, N 14.11. IR (KBr) (ν_{max}/cm^{-1}: 2923 (m), 1579 (vs), 1508 (vs), 1474 (m), 1438 (s), 1275 (vs), 1240 (vs), 1007 (m), 840 (s), 818 (m), 770 (s) and 546 (s).

Table 1 Crystallographic data for **1** and **2**

	1	**2**
Chemical Formula	$C_{24}H_{19}Cl_2FeN_6O_{4.5}$	$C_{24}H_{19}Cl_2MnN_6O_{4.5}$
FW/g mol^{-1}	590.20	589.29
Space group	$P2_1/c$	$P2_1/c$
a/Å	12.5743(9)	12.5083(3)
b/Å	14.0029(6)	14.1086(4)
c/Å	15.1688(10)	15.2964(4)
β/°	113.043(4)	112.822(3)
V/Å	2457.8(3)	2488.10(11)
Z	4	4
T/K	100(2)	100(2)
ρ_c/g cm^{-3}	1.595	1.573
Reflections collected/$2\theta_{max}$	12 052/50.00	45 198/63.06
Unique reflections	4308	8287
R_{int}	0.0403	0.0512
No. of parameters	343	343
λ/Å/μ/mm^{-1}	0.71073/0.878	0.71073/0.792
R_1[a]/GOF[b]	0.0389/1.037	0.0427/1.019
[c]wR_2 ($I > 2\sigma(I)$)	0.0736	0.0986
Residual density/e Å^{-3}	+0.44/–0.34	+1.103/–0.98

Observation criterion: $I > 2\sigma(I)$. [a] $R_1 = \Sigma \| F_o | - | F_c \| / \Sigma | F_o |$. [b] GOF = $\{\Sigma[w(F_o^2 - F_c^2)^2]/(n-p)\}^{1/2}$, [c] w$R_2 = [\Sigma[w(F_o^2 - F_c^2)2]/\Sigma[w(F_o^2)^2]]^{1/2}$ where w = $1/[\sigma^2(F_o^2) + (aP)^2 + bP]$, $P = (F_o^2 + 2F_c^2)/3$.

X-Ray crystallographic data collection and refinement of the structures

Single crystals of **1** (green) and **2** (orange) were picked up with nylon loops and were mounted in the nitrogen cold stream of the diffractometer. Final cell constants were obtained from least squares fits of all measured reflections. Intensity data were corrected for absorption using intensities of redundant reflections. The structures were readily solved by direct methods and subsequent difference Fourier techniques. The crystallographic data of **1** and **2** are listed in Table 1. The Siemens SHELXTL[21a] software package was used for solution and artwork of the structure, SHELXL-97[21b] was used for the refinement. All non-hydrogen atoms were refined anisotropically. Hydrogen atoms, except hydrogen atoms of the solvate water molecules, were placed at calculated positions and refined as riding atoms with isotropic displacement parameters. A water molecule of crystallization forms hydrogen bonds to coordinated chloride ions of two neighbouring complex molecules in isostructural complexes **1** and **2**. The water molecule was found to be disordered next to a crystallographic inversion centre. The oxygen atom was therefore refined with an occupation factor of 0.5. Due to this disorder, location of hydrogen atoms was not successful.

Density functional theory (DFT) calculations

All calculations reported in this article were done with the Gaussian 03W[22] programme package supported by GaussView 4.1. The DFT[23] and TDDFT[24] calculations have been performed at the level of Becke three parameter hybrid functional with the non-local correlation functional of Lee–Yang–Parr (B3LYP)[25] In gas-phase, the geometry of **1** on X-ray coordinates, but geometries of $(L^{\phi})_2Fe^{II}Cl_2$ (**3**), and $(bpy)_2Fe^{II}Cl_2$ (**4**)[18b,c] on theoretical coordinates have been optimized using Pualy's Direct Inversion[26] in the Iterative Subspace (DIIS), 'tight' convergent SCF procedure[27] ignoring symmetry. The DFT calculations of **2** have been carried out using single crystal X-ray structural coordinates. In all calculation, a LANL2DZ basis set along with the corresponding effective core potential (ECP) was used for iron or manganese metal atoms.[28–30] Basis set 6-31G[31] for H has been used. For non-hydrogen atoms first polarization functions have been added. Basis set 6-31G(d,p)[32] for C, N, O and 6-311G(d,p)[33] for Cl atoms are employed for the calculation of **1**, **2**, and **3**. For **4**, we faced problem and have incorporated both polarization and diffusion functions. Basis set 6-31++G**[31b,34] for C and N atoms has worked successfully to converge in SCF. To compare the ground state energies and ligand orientations, the geometries of *ccc*, *ttt*, *cct* and *ctc* isomers of iron have been optimized using DIIS and 'tight' convergence in SCF. The geometry of *cct* isomer failed to converge because of crowding and unexpected bonding interactions. The percentage contribution of metal, chloride and ligands of the frontier orbitals of **1** (g), have been calculated using GaussSum programme package.[35] The sixty lowest singlet excitation energies on the optimized geometry of **1** (g) in methanol have been calculated by TDDFT method using conductor-like polarisable continuum model (CPCM).[36] The nature of transitions has been calculated by adding the probability of same type among alpha and beta molecular orbitals.

Results and discussion

Syntheses of complexes

Pre-isolation of pure aldimine ligand, (*E*)-3-nitro-*N*-(pyridine-2-ylmethylene)aniline ($L_{NO_2}{}^{\phi}$) did not succeed. But to study, the emission properties of the ligand backbone, (*E*)-4-hydroxy-*N*-(pyridine-2-ylmethylene)aniline (L_{OH}) ligand has been isolated in good yield and characterized. The L_{OH} ligand does not afford any product with Fe(II) or Mn(II) metal ions. Two *tcc*-isomers of iron and manganese isolated in this work with $L_{NO_2}{}^{\phi}$ ligand, are shown in Fig. 1 and 2 (*tcc* refers to *trans–cis–cis* positions with respect to pyridine N-imine N–Cl donors). Two unsymmetrical diimine ligands in these complexes are non-equivalent which are defined as $L_{NO_2}{}^{\phi}$ (ϕ = dihedral angle between the diimine unit including pyridine ring and phenyl ring planes). The complexes are abbreviated as $(L_{NO_2}{}^{\phi 1})(L_{NO_2}{}^{\phi 2})M^{II}Cl_2$ where ϕ_1, ϕ_2 are dihedral angles for two different diimine ligands. The crystalline compounds of **1** and **2** with water as a solvent of crystalization have been prepared in high yield in a single step reaction of 2-pyridinecarbaldehyde, 3-nitroaniline and hydrated metal dichloride in methanol at room temperature. Yield of **1** is higher in anaerobic environment. Reaction of 2-pyridinecarbaldehyde with aniline in similar condition does not afford any product. We failed to isolate any product with 2-nitro or 4-nitroanilines. It is noteworthy that in both cases, with $L_{NO_2}{}^{\phi}$, only *tcc*-isomer of possible five stereoisomers crystallizes from the reaction mixtures.

Table 2 Selected bond lengths (Å) and angles (°) of **1** and **2**

1		**2**	
Fe1–N1	2.195(2)	Mn1–N1	2.2759(15)
Fe1–N21	2.187(2)	Mn1–N21	2.2843(16)
Fe1–N8	2.298(2)	Mn1–N8	2.4176(15)
Fe1–N28	2.234(2)	Mn1–N28	2.3300(15)
Fe1–Cl40	2.4394(8)	Mn1–Cl1	2.4496(6)
Fe1–Cl50	2.3449(8)	Mn1–Cl2	2.4012(5)
N1–Fe1–N21	163.54(9)	N1–Mn1–N21	161.68(6)
N28–Fe1–Cl50	162.92(7)	N28–Mn1–Cl2	157.90(4)
N8–Fe1–Cl40	164.29(7)	N8–Mn1–Cl1	161.41(4)
Cl50–Fe1–Cl40	100.27(3)	Cl2–Mn1–Cl1	103.82(2)

Molecular structures

Single-crystal X-ray structure determinations at 100 K have confirmed the *tcc* geometry of **1** and **2**. Molecular geometries of the species in crystals have been shown in Fig. 1 and 2. Selected bond parameters of **1** and **2** are listed in Table 2. In **1**, the average Fe–N (pyridine) distance, 2.190(2) Å is shorter than the average Fe–N(imine) distance, 2.266(2) Å. These bond parameters are comparable to those of $Fe(phen)_2Cl_2$. The Cl–Fe–Cl angle in $Fe(phen)_2Cl_2$, 100.26(3)° is similar to that in **1**.

But the supramolecular chemistry of **1** (illustrated below) contrasts $Fe(phen)_2Cl_2$ in which only the π–π stacking has been evidenced.[18a] The similar features have been observed in **2**. The Mn(II)–N(pyridine) distance is shorter than the average Mn–N(imine) distances, 2.3738(15). In all three cases, two *cis*-M–Cl distances are not equal. The most important feature is that the two diimines in the crystals of **1** and **2** are non-equivalent which are defined by ϕ. In **1**, two diimine ligands are $L_{NO_2}{}^{33.6}$ and $L_{NO_2}{}^{79.3}$ as in Fig. 3. In **1**, the diimine unit including the pyridine ring (A) of $L_{NO_2}{}^{33.6}$ forms a good plane of mean deviation around 0.01 Å. In $L_{NO_2}{}^{79.3}$, the mean deviation of the plane of the diimine fragment with the pyridine ring (C) is about 0.05 Å. The orientations of the two ligands in **2** are very similar to **1**. In **2**, two diimine ligands are $L_{NO_2}{}^{32}$ and $L_{NO_2}{}^{79.4}$. In **1** and **2**, the π^* orbitals respectively of $L^{79.3}$ and $L^{79.4}$ ligands will be more destabilized compared to $L_{NO_2}{}^{33.7}$ (Chart 2) leading to distinct UPMOs. In lattice, such molecular orientation has been forced to avoid the interaction between the two aromatic rings. To minimize the crowding, pyridine (A) and the 3-nitrophenyl (D) rings remain parallel. The distance between

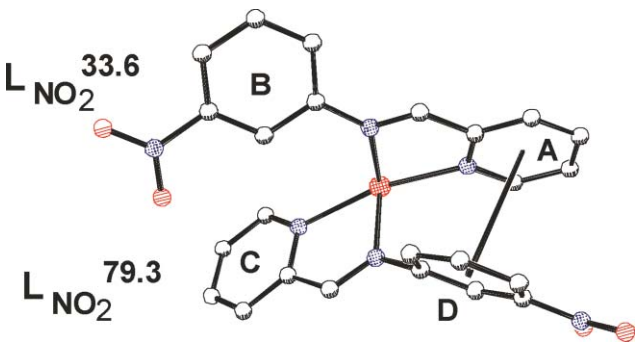

Fig. 3 Non-equivalent orientations of two diimine ligands of **1** in crystals.

Table 3 Significant weak bonding distances (Å) in crystals of **1**

O17–N15	2.901	H5–Cl40	2.739
O36–N15	2.953	H12–Cl50	2.663
H4–O17	2.445	H23–Cl40	2.839
H24–O36	2.516	H27–Cl50	2.659
H10–O(HOH)	2.363	O(HOH)–Cl40	2.967
H34–O(HOH)	2.392	H7–O(HOH)	2.333

Table 4 Significant weak bonding distances (Å) in crystals of **2**

O16–N15	2.867	H5–Cl1	2.734
O37–N15	2.940	H12–Cl2	2.651
H4–O16	2.429	H32–Cl2	2.302
H24–O37	2.482	H27–Cl2	2.659
H7–O(HOH)	2.327	O(HOH)–Cl40	2.871
H30–O(HOH)	2.302		

the centres of these two rings is 3.589 and 3.962 Å respectively for **1** and **2**.

Non-bonding assemblies

Out of the possible five stereo-isomers, *i.e.*, *tcc*, *ctc*, *ccc*, *ttt*, *cct*, the reaction mixtures afford only well-shaped isolable crystals of the *tcc*-isomers as the products which display strong intermolecular non-bonding interactions furnishing 2D and 3D assembly. The non-bonding assemblies have been realized because of the (i) pendent NO_2–NO_2 (ii) NO_2–H (aromatic) (iii) *cis*-MCl_2–HOH(solvent) (iv) *cis*-MCl_2–H(aldimine) (v) *cis*-MCl_2–H(aromatic) and (vi) HOH–H non-bonding interactions. The different types of effective intermolecular non-bonding lengths of **1** have been listed in Table 3.

The interligand H-bonding among aromatic hydrogen atoms and -NO_2 groups results the H-bonded double-stranded orientation of the coordinated diimine ligands which are wrapped around and helical with respect to Fe(II)–Fe(II) axes forming dinuclear double-stranded helical assembly as in Fig. 4. A weak bonding centro-symmetric [2 × 2] grid type assembly has been the building blocks of the 3D architecture of **1**. The dipole of the hanging –NO_2 group at the 120° angle of the aldimine function interacts with the dipole of the -NO_2 group of another molecule and generates a novel [2 × 2] parallelogram (Fe–Fe = 12.574 and 11.523 Å, Fe–Fe–Fe = 118 and 62°) grid (**1a**) as in Fig. 5. The assembly **1a** is interlinked *via* Cl atoms and H_2O molecules as in Fig. 5 (Fe–Fe = 9.504 Å, Fe–Fe–Fe = 138.9 and 41.1°) constructing 2D assemblies which are helical in nature and assemble to a channelled 3D architecture by strong inter-helices H-bonding interactions. Similar to iron, the non-covalent tetranuclear [2 × 2] parallelogram (Mn–Mn = 12.508 and 11.767 Å, Mn–Mn–Mn = 117.7 and 62.3°) grid has been stabilized as in Fig. 6. This tetranuclear assembly of manganese is the building block of the 3D architecture of **2**. The different types of effective intermolecular non-bonding lengths have been listed in Table 4. The assembly is interlinked *via* Cl atoms and H_2O molecules as in Fig. 5 constructing 2D assemblies which are helical in nature and results to a channelled 3D architecture by strong inter-helices H-bonding interactions.

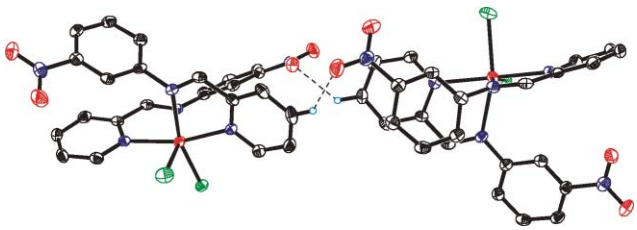

Fig. 4 Double-stranded dinuclear helices in **1**.

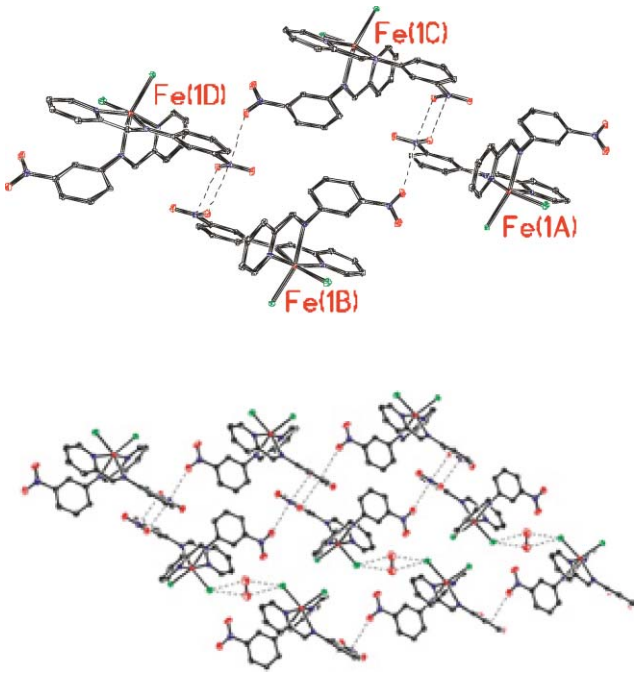

Fig. 5 Centrosymmetric $L_8Fe_4Cl_8$ assembly (**1a**) of **1** (top) and self assembling of **1a** with H_2O along a particular plane (bottom) extracted from the packing diagram along *a* axis.

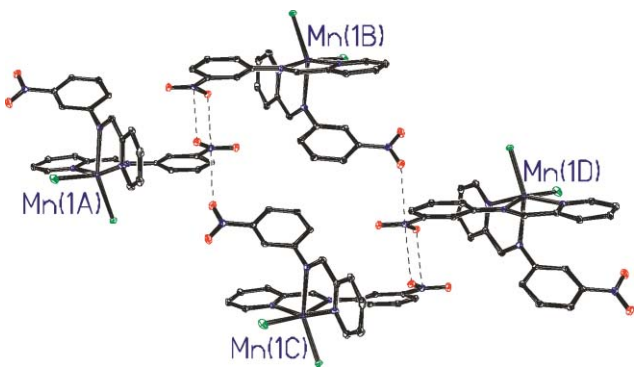

Fig. 6 Centrosymmetric $L_8Mn_4Cl_8$ assembly of **2**.

Gas phase geometry

Orientations of the two unsymmetrical diimines in the crystals have already been confirmed by single-crystal X-ray structure determinations of **1** and **2**. Geometries of all possible isomers of iron in gas-phase have been optimized at the DFT/B3LYP level of the theory. The important finding is that the non-equivalence of the two diimine ligands in *tcc*-isomer prevails in gas phase also. In the optimized geometry of the isomer, the orientations of the two aryl rings around ═N–C bond are different with $\phi_1 = 42°$ and $\phi_2 = 61°$. Thus, in gas phase, **1** is defined as **1** (g), $(L_{NO_2}{}^{42})(L_{NO_2}{}^{61})Fe^{II}Cl_2$.

Calculations have also established that compared to *ttt*, *ctc* and *ccc* isomers, **1** (g) is stabilized at least by 5.5, 12.7 and 23.1 kJ mol^{-1}, respectively, as in Scheme 1. The minimum energy of the *tcc* isomer in gas-phase correlates well with the experimental finding of the isolated product. Further, the luminescence and lifetime data of the species in methanol glasses as given below, predict the presence of only one isomer in solution too. Moreover, it is to be noted that the two diimine ligands only in **1** (g) are non-equivalent. In all other *ttt*, *ccc*, *ctc* isomers, the two ligands are equivalent (Scheme 1). We failed to isolate any metal complexes without the nitro group in the ligand. But to calibrate the effect of the nitro group, we have optimized the structure *tcc*-FeL_2Cl_2 (**3**), by a similar method. It is found that the two diimine ligands in **3** are equivalent as in $Fe(bpy)_2Cl_2$ (**4**). In **3**, both the aryl rings are rotated only by 46° with respect to the diimine fragment and both the ligands are abbreviated as L^{46}. Unfortunately, due to strong interaction between two aryl rings approaching to bonding distances, *cct* isomer fails to converge in SCF and it appears to be the least stable. It concludes that the non-equivalence is the selectivity of these bis(unsymmetrical diimine) species in solids and even, in gas phase.

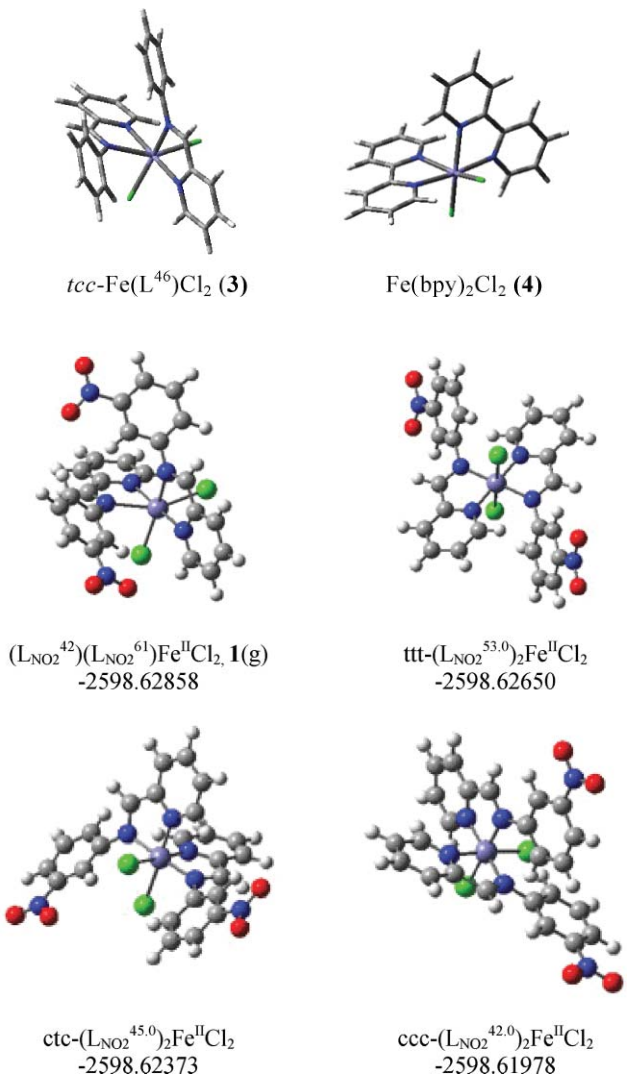

Scheme 1 Optimized geometries and energies (a.u.) of possible isomers of iron in gas phase.

Mössbauer spectra and magnetic measurements

Quadrupole splitting in Mössbauer spectra is a shift in nuclear energy levels that is induced by an electric field gradient caused by nearby electrons, *i.e.* coordinated ligands.[37] Different isomers with different dipole moment, of course, produce different electric field gradient resulting in different quadrupole splitting. The combination of isomer shift and quadrupole splitting is thus used to identify the valence state and site occupancy of a Mössbauer active element in complexes and has been a tool to follow isomerization.[38] For octahedral iron complexes, it was reported that the quadrupole splitting of a *trans*-isomer is twice of that of a *cis*-isomer.[39]

Only one doublet in Zero field Mössbauer spectrum at 80 K of **1** (Fig. 7) has prompted the presence of one pure stereoisomer and the identical iron centers in the isolated bulk compound. Isomer shift, 1.096 mm s^{-1} and the quadruple splitting, 3.055 mm s^{-1} parameters are corroborated with the iron(II) high spin state. Variable-temperature SQUID were performed on powder samples and the temperature independent magnetic susceptibilities at the range of 40–200 K clearly correspond to the ground state of total spin $S = 2$ for **1** as in Fig. 8 and $S = 5/2$ for **2**. Thus, all these complexes belong to high spin dihalobis(diimine)M(II) family.

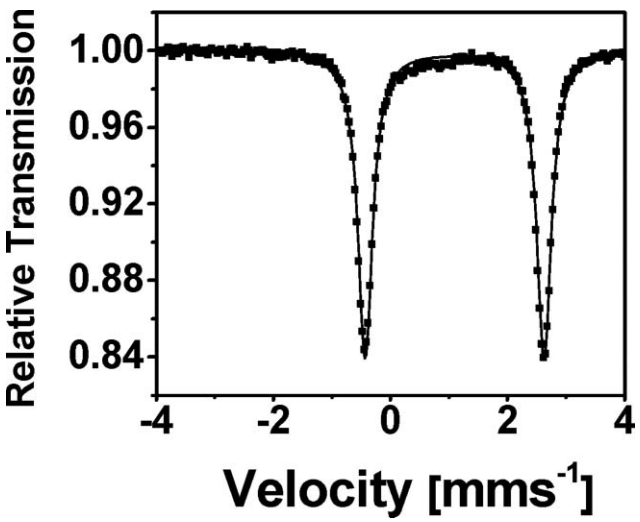

Fig. 7 Zero-field Mössbauer spectrum of bulk sample of **1** at 80 K.

Photophysical properties

The absorption and emission spectral data of **1** and **2** in methanol have been summarized in Tables 5 and 6. Absorption spectra are shown in Fig. 9(a). All these complexes display very strong absorption bands at 300–200 nm and moderately strong band at above 300 nm. The absorption feature of these species is solvent

Table 5 UV-vis spectral data of **1** and **2** in MeOH and CH_2Cl_2 solvents

Compound	Solvent	λ_{max}/nm (ε/$M^{-1}cm^{-1}$)
1	MeOH	425 (7250), 348 (9900), 246 (18 850)
	CH_2Cl_2	318 sh (28 920)
2	MeOH	366 (4110), 259 (56 510), 203 (35 000)
	CH_2Cl_2	322 sh (28 690)

Table 6 Excitation (λ_{ex}), emission (λ_{em}) maxima and luminescence lifetimes of **1** and **2** in frozen MeOH glasses at 77 K

Compound	λ_{ext}/nm	λ_{em}/nm	Lifetime/ns (λ_{ext} at 356 nm)	χ^2	τ_{av}/ns
1	370	521	τ_1 = 6.8 (3.0%) τ_2 = 0.44 (97.0%)	1.3	0.57
2	368	524	τ_1 = 9.7 (2.8%) τ_2 = 0.65 (97.2%)	1.1	0.90

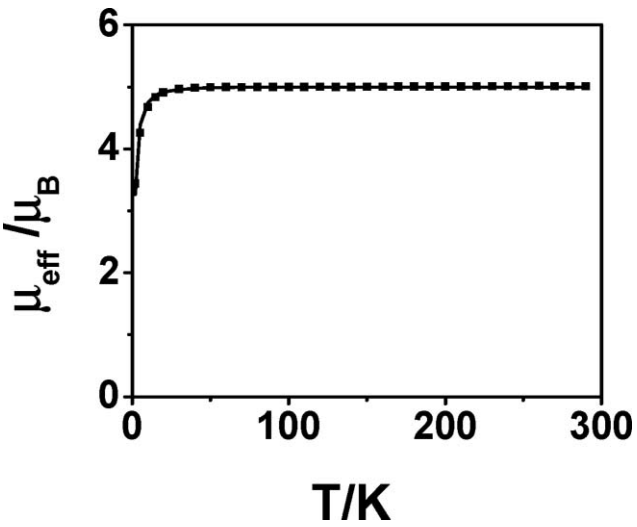

Fig. 8 Variable-temperature magnetic moment, μ_{eff}, μ_B, of **1**.

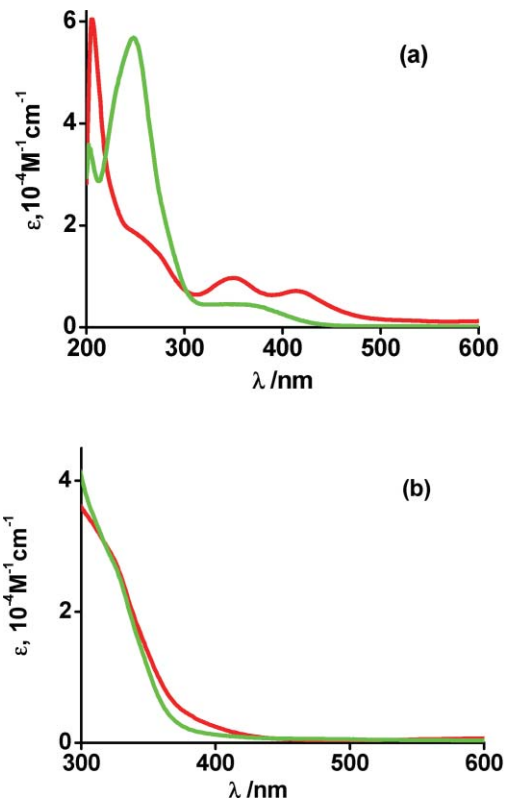

Fig. 9 UV-vis spectra of **1** (red), **2** (green) in (a) MeOH (b) CH_2Cl_2.

dependent. In dichloromethane solvent, the absorption spectra are not well structured as in methanol. The spectra in dichloromethane have been shown in Fig. 9(b). It evidently shows that absorption feature of **1** and **2** in dichloromethane is metal independent. The low energy band above 350 nm is missing in dichloromethane solvent.

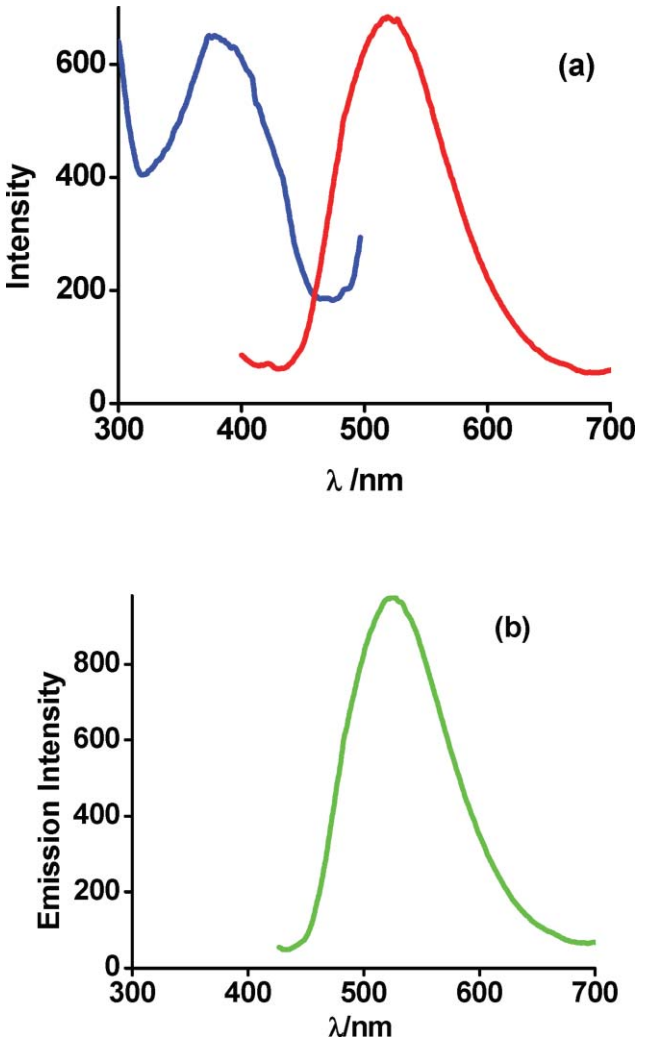

Fig. 10 (a) Excitation (blue), emission (red) spectra of **1** and (b) emission spectrum of **2** (green) in frozen MeOH glasses at 77 K.

In contrast to $(bpy)_2FeCl_2$ and $(phen)_2FeCl_2$, compounds **1** and **2** are luminescent. Emission spectra of the frozen methanol glasses with the concentration in the order of 10^{-5} mol L^{-1} have been recorded at 77 K with λ_{ext} at 370 and 368 nm (Table 6) for **1** and **2**. The luminescence spectra are displayed in Fig. 10. The luminescence lifetimes of the species have been measured exciting at 356 nm. The data has been fitted well with the one component more than 97%. All these parameters do not imply presence of any other isomers in solution.

The compounds are not luminescent in dichloromethane–toluene glasses. We failed to isolate the free L_{NO_2} ligand but the emission property of the ligand backbone has been investigated with the isolated L_{OH} ligand. It is observed that the free L_{OH} ligand is not emissive in solid, solutions even at 77 K. The origins of the absorption and luminescence of **1** and **2** have been elucidated by TD-DFT calculations and the results have been described below.

Localization of LUMOs and excited states

Ground state electronic structure and features of the molecular orbitals of **1** have been analyzed by density functional theory calculations at the unrestricted B3LYP level. The geometry of **1** in gas-phase was optimized with quintet spin state without any symmetry constraint using tight convergence in SCF. The bond parameters of the optimized structure are as follows: Fe–N (Py) = 2.263, 2.253; Fe–N(imine) = 2.351, 2.387; Fe–Cl = 2.440, 2.392; –CH═N– = 1.281, 1.282;–CH═N(Py) = 1.351, 1.350; ═CH–C(Py) = 1.466, 1.465 Å. The calculated bond lengths of the coordination sphere differ significantly from the experimental single crystal structure which displays strong non-bonding intermolecular interactions. The other bond parameters of the ligand correlate well with the experimental bond distances. The spin density distribution of optimized molecule of **1** is as follows: Fe, 3.68; Cl, 0.096; N, 0.05 which are consistent with the Fe(II) high spin state.

The calculation has established the structure of the UPMOs. It has summed up the effect of the two non-equivalent diimine ligands. Two halves of a ligand behave independently and two ligands construct four closely spaced localized unoccupied molecular orbitals as in Fig. 11. The alpha LUMO is localized on the less conjugated $L_{NO_2}{}^{61}$ ligand while the beta LUMO is localized on $L_{NO_2}{}^{42}$ ligand. The alpha LUMO + 1 is composed of $L_{NO_2}{}^{42}$ ligand but the beta LUMO + 1 is composed of $L_{NO_2}{}^{61}$.

Effect of non-equivalence of two coordinated diimines has also been noted in the LUMO + 2 and LUMO + 3 orbitals. The alpha LUMO + 2 and LUMO + 3 are localized respectively on $L_{NO_2}{}^{42}$ and $L_{NO_2}{}^{61}$ ligands but the prime components of beta LUMO + 2 and LUMO + 3 are $L_{NO_2}{}^{42}$ and $L_{NO_2}{}^{61}$ ligands. Beta HOMO is an iron d-orbital while alpha HOMO and HOMO – 1 have mixed origins.

The structure of UPMO is different in **3**. In compared to **1**, compound **3**, has only two closely spaced unoccupied molecular orbitals that are delocalized over two diimine ligands. LUMO and LUMO + 1 are equally distributed over the two diimine ligands. Each of the diimine ligands contributes 48–50% to the LUMO and LUMO + 1 (alpha and beta) orbitals. Thus, both the first and second excited states are delocalized over two diimine ligands. Similar structure of the UPMOs has been noted in non-emissive $(bpy)_2FeCl_2$ (**4**) where two bpy ligands are equivalent. Two low-lying π^* orbitals of **4** are delocalized over two bpy ligands. With the two non-equivalent diimine ligands and nitro substituents complexes **1** and **2** are different. They possess lower symmetry which prompts the localized excited state with higher transition dipole moment change ($\Delta\mu \neq 0$) with higher probability of absorption.

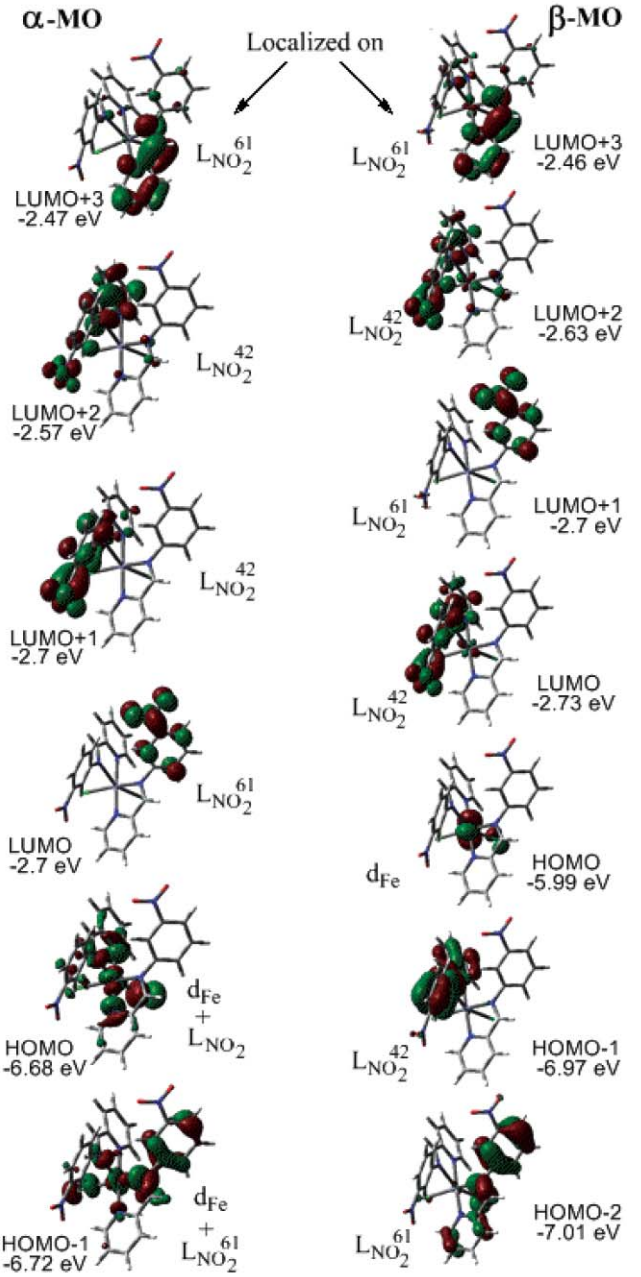

Fig. 11 Localized photoactive alpha and beta molecular orbitals of **1** (g) (isosurface value 0.04).

Excitation energies

To elucidate the origin of the luminescence of **1** and **2**, TD-DFT calculations were carried out on **1** in methanol using CPCM model. The transition types of the lower energy absorption maxima are summarized in Table 7. Analyses have found out two types of transitions for the absorptions. These are metal to ligand charge transfer (MLCT) and intraligand (IL) or ligand to ligand charge transfer (LLCT). Excitation energies of the transitions with oscillator strength greater than 0.015 for the above 340 nm have been tabulated. As the range of excitation wavelength for the emission is 340–370 nm, the absorption peak at 348 nm (λ_{max}) or longer wavelength is worthy investigating. The origin of calculated bands at 345.97 nm ($f = 0.024$) and 346.52 nm ($f = 0.017$) has given an insight of the origin of the transition of the experimental band at 348 nm. Simulation of the absorption spectrum from the output file of the TD-DFT calculations of **1** in methanol has been shown in Fig. 12 which displays similar features of the experimental spectrum (Fig. 9(a)).

It is important to assign the origin of the observed low energy broad band in the range of 400–490 nm with the maxima at 425 nm of **1**. TD calculation of **1** has found a weak band at 485 nm (f = 0.0084) the origin of which is MLCT (Table 7). The analyses have

Table 7 Excitation maxima (nm), oscillator strength (f) of dominant transitions types with probabilities (>5%) from TD-DFT calculation of **1** in methanol

λ_{cal}/nm (f)	Significant contributions	Dominant type
486.30 (0.008)	β HOMO → LUMO (61%)	$d_{Fe} \rightarrow \pi^*(L_{NO_2}{}^{42})$
	β HOMO → LUMO + 2 (15%)	$d_{Fe} \rightarrow \pi^*(L_{NO_2}{}^{42})$
	β HOMO → LUMO + 4 (15%)	$d_{Fe} \rightarrow d_{Fe}$
346.52 (0.017)	α HOMO − 1 → LUMO + 1 (6%)	$d_{Fe} + \pi(L_{NO_2}{}^{61}) \rightarrow \pi^*(L_{NO_2}{}^{42})$
	α HOMO → LUMO (12%)	$d_{Fe} + L_{NO_2} \rightarrow \pi^* (L_{NO_2}{}^{61})$
	α HOMO → LUMO + 1 (14%)	$d_{Fe} + L_{NO_2} \rightarrow \pi^* (L_{NO_2}{}^{42})$
	β HOMO − 2 → LUMO + 1 (50%)	$\pi(L_{NO_2}{}^{61}) \rightarrow \pi^* (L_{NO_2}{}^{61})$
345.97 (0.024)	α HOMO − 1 → LUMO (21%)	$d_{Fe} + \pi(L_{NO_2}{}^{61}) \rightarrow \pi^* (L_{NO_2}{}^{61})$
	α HOMO − 1 → LUMO + 1 (11%)	$d_{Fe} + \pi(L_{NO_2}{}^{61}) \rightarrow \pi^*(L_{NO_2}{}^{42})$
	α HOMO − 1 → LUMO + 2 (7%)	$d_{Fe} + \pi(L_{NO_2}{}^{61}) \rightarrow \pi^* (L_{NO_2}{}^{42})$
	β HOMO − 1 → LUMO (25%)	$\pi(L_{NO_2}{}^{42}) \rightarrow \pi^*(L_{NO_2}{}^{42})$
	β HOMO − 1 → LUMO + 2 (8%)	$\pi(L_{NO_2}{}^{42}) \rightarrow \pi^*(L_{NO_2}{}^{42})$

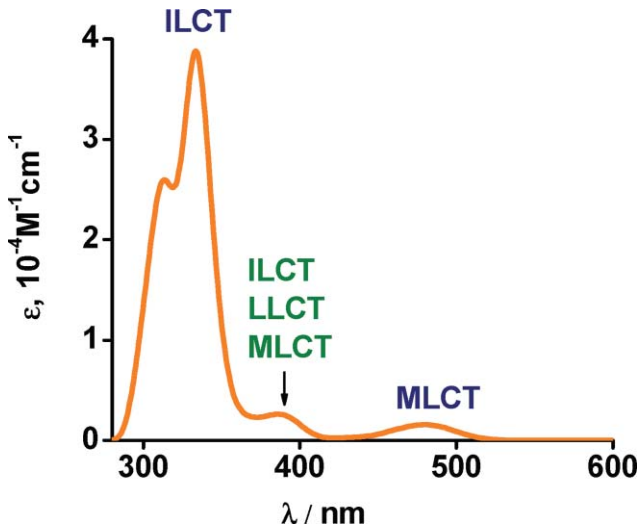

Fig. 12 Simulated electronic spectrum from TD-DFT calculation of **1** in methanol.

shown that inter- and intra- ligand charge transfers are the major contributions of the two calculated absorption maxima at 346 nm (Table 7). The lower energy absorptions at higher than 340 nm thus have mixed MLCT, ILCT and LLCT origins which are absent in less polar non-protic solvent (Fig. 9(b)) and the compounds have accordingly been found to be non-emissive in dichloromethane solutions.

The calculations further have inferred that relatively higher energy absorptions at less than 330 nm are mainly due to ILCT transitions. As it has already been established that the UPMOs are localized, the MLCT and IL or LLCT excited states are expected to be solvent dependent that is observed in the experimental spectra. Again, the luminescence features of the species have been found to be metal independent. On the basis of these analyses, IL and LLCT dominated excited states at 350–370 nm with a shorter luminescence life time have been assigned to the origin of emission for these species.

The molecular geometry of **2** has not been optimized and all calculations have been done on single-crystal X-ray structural coordinates. The frontiers unoccupied orbitals of these species display similar features of localization as in **1** in methanol solution.

Conclusion

A single, optically active isomer of bis(unsymmetrical diimine)MCl_2 (M = Fe, Mn) family has been isolated in the solid state and substantiated by various experimental techniques. DFT calculations have established the lowest ground state energy of the *tcc*-isomer in gas phase too. Because of the non-equivalence of two diimine ligands, these isomers produce a band of four closely spaced UPMOs that are localized. In contrast, the calculations have established that two diimine ligands of *ttt*, *ccc*, *ctc* isomers in gas-phase are equivalent and form delocalized UPMO as in non-emissive $(bpy)_2FeCl_2$ species. The complexes of iron and manganese reported here are high spin but luminescent in frozen methanol glasses at 77 K because of ILCT and LLCT dominated excited state. Thus, co-ordination of unsymmetrical diimine ligands to 3d metal ions constituting an origin of photoluminescence is well worth investigating.

Acknowledgements

We are thankful to the Council of Scientific and Industrial Research (CSIR), New Delhi, (01(1957)/04/EMR-II) and DST (SR/SI/IC/10/2008) for financial support. We are grateful to Ramakrishna Mission, Belur Math for funding the Luminescence Spectrometer. A. S. R gratefully acknowledges CSIR for SRF (8/531(001)2008-EMR-I).

References

1 (*a*) P. A. Liddell, D. Barrett, L. R. Makings, P. J. Pessiki, D. Gust and T. A. Moore, *J. Am. Chem. Soc.*, 1986, **108**, 5350–5352; (*b*) D. Gust, T. A. Moore, L. R. Makings, P. A. Liddell, G. A. Nemeth and A. L. Moore, *J. Am. Chem. Soc.*, 1986, **108**, 8028–8031; (*c*) P. Seta, E. Bievenue, A. L. Moore, P. Mathis, R. V. Bensasson, P. Liddell, P. J. Pessiki, A. Joy, T. A. Moore and D. Gust, *Nature*, 1985, **316**, 653; (*d*) D. Kuciauskas, P. A. Liddell, S. C. Hung, S. Lin, S. Stone, G. R. Seely, A. L. Moore, T. A. Moore and D. Gust, *J. Phys. Chem. B*, 1997, **101**, 429–440; (*e*) G. Steinberg-Yfrach, P. A. Liddell, S. C. Hung, A. L. Moore, D. Gust and T. A. Moore, *Nature*, 1997, **385**, 239–241; (*f*) D. Gust, *Nature*, 1997, **386**, 21–22.
2 M. R. Wasielewski, *Chem. Rev.*, 1992, **92**, 435–461.
3 C. S. Kraemer and T. J. Mueller, *Eur. J. Org. Chem.*, 2003, 3534–3548.
4 D. M. Kaschak, J. T. Leau, C. C. Waraksa, G. B. Saupe, H. Usami and T. E. Mallouk, *J. Am. Chem. Soc.*, 1999, **121**, 3435–3445.
5 T. J. Meyer, *Acc. Chem. Res.*, 1989, **22**, 163.
6 (*a*) J. Schneider, P. Du, X. Wang, W. W. Brennessel and R. Eisenberg, *Inorg. Chem.*, 2009, **48**, 1498; (*b*) R. Eisenberg and D. G. Nocera, *Inorg.*

Chem., 2006, **45**, 1880; (*c*) S. Chakraborty, T. J. Wadas, H. Hester, R. Schmehl and R. Eisenberg, *Inorg. Chem.*, 2005, **44**, 6865.
7 M. D. Ward, *Coord. Chem. Rev.*, 2006, **250**, 3128.
8 (*a*) C. J. Adams, N. Fey, Z. Harrison, I. V. Sazanovich, M. Towrie and J. A. Weinstein, *Inorg. Chem.*, 2008, **47**, 8242; (*b*) C. J. Adams, N. Fey and J. A. Weinstein, *Inorg. Chem.*, 2006, **45**, 6105.
9 J. Bossert and C. Daniel, *Coord. Chem. Rev.*, 2008, **252**, 2493.
10 D. J. Stufkens and A. Vlcek, *Coord. Chem. Rev.*, 1998, **177**, 127.
11 K. A. O'Donoghue, J. M. Kelly and P. E. Kruger, *Dalton Trans.*, 2004, 13.
12 (*a*) A. S. Roy, N. Muresan, H. M. Tuononen, S. P. Rath and P. Ghosh, *Dalton Trans.*, 2008, 3438; (*b*) A. S. Roy, H. M. Tuononen, S. P. Rath and P. Ghosh, *Inorg. Chem.*, 2007, **46**, 5942.
13 See, for example: (*a*) R. J. Baker, R. D. Farley, C. Jones, D. P. Mills, M. Kloth and D. M. Murphy, *Chem.–Eur. J.*, 2005, **11**, 2972; (*b*) M. Kaupp, H. Stoll, H. Preuss, W. Kaim, T. Stahl, G. Van Koten, E. Wissing, W. J. J. Smeets and A. L. Spek, *J. Am. Chem. Soc.*, 1991, **113**, 5606; (*c*) T. Pott, P. Jutzi, B. Neumann and H. G. Stammler, *Organometallics*, 2001, **20**, 1965; (*d*) C. Corvaja and L. Pasimeni, *Chem. Phys. Lett.*, 1976, **39**, 261; (*e*) S. Richter, C. Daul and A. Zelewsky, *Inorg. Chem.*, 1976, **15**, 943.
14 (*a*) K. Nozaki, K. Takamori, Y. Nakatsugawa and T. Ohno, *Inorg. Chem.*, 2006, **45**, 6161; (*b*) E. M. Kober and T. J. Meyer, *Inorg. Chem.*, 1982, **21**, 3967; (*c*) J. Ferguson and F. Herren, *Chem. Phys.*, 1983, **76**, 45; (*d*) E. M. Kober and T. J. Meyer, *Inorg. Chem.*, 1984, **23**, 3877; (*e*) L. Karki and J. T. Hupp, *Inorg. Chem.*, 1997, **36**, 3318; (*f*) D. W. Thompson, C. N. Fleming, B. D. Myron and T. J. Meyer, *J. Phys. Chem. B*, 2007, **111**, 6930; (*g*) E. Danielson, C. M. Elliott, J. W. Merkert and T. J. Meyer, *J. Am. Chem. Soc.*, 1987, **109**, 2519; (*h*) K. A. Maxwell, M. Sykora, J. M. Desimone and T. J. Meyer, *Inorg. Chem.*, 2000, **39**, 71; (*i*) N. Nickita, M. J. Belousoff, A. I. Bhatt, A. M. Bond, G. B. Deacon, G. Gasser and L. Spiccia, *Inorg. Chem.*, 2007, **46**, 8638; (*j*) J. P. Paris and W. W. Brandt, *J. Am. Chem. Soc.*, 1959, **81**, 5001; (*k*) Jr. J. L. Zambrana, E. X. Ferloni, J. C. Colis and H. D. Gafney, *Inorg. Chem.*, 2008, **47**, 2; (*l*) D. Kotkar, V. Joshi and P. K. Ghosh, *Inorg. Chem.*, 1986, **25**, 4334.
15 (*a*) S. Chakraborty, T. J. Wadas, H. Heidi Hester, C. Flaschenreim, R. Schmehl and R. Eisenberg, *Inorg. Chem.*, 2005, **44**, 6284; (*b*) T. J. Wadas, S. Chakraborty, R. J. Lachicotte, Q.-M. Wang and R. Eisenberg, *Inorg. Chem.*, 2005, **44**, 2628; (*c*) J. Schneider, Y.-A. Lee, J. Pérez, W. W. Brennessel, C. Flaschenriem and R. Eisenberg, *Inorg. Chem.*, 2008, **47**, 957; (*d*) Y. Scaffidi-Domianello, A. A. Nazarov, M. Haukka, M. Galanski, B. K. Keppler, J. Schneider, P. Du, R. Eisenberg and V. Y. Kukushkin, *Inorg. Chem.*, 2007, **46**, 4469; (*e*) Q.-M. Wang, Y.-A. Lee, O. Crespo, J. Deaton, C. Tang, H. J. Gysling, M. C. Gimeno, C. Larraz, M. D. Villacampa, A. Laguna and R. Eisenberg, *J. Am. Chem. Soc.*, 2004, **126**, 9488; (*f*) D. Amarante, C. Cherian, A. Catapano, R. Adams, M. H. Wang and E. G. Megehee, *Inorg. Chem.*, 2005, **44**, 8804.
16 J. N. Demas and B. A. DeGraff, *Anal. Chem.*, 1991, **63**, 829A.
17 (*a*) P. Yang, B. C. K. Chan and M. C. Baird, *Organometallics*, 2004, **23**, 2752–2761; (*b*) B. P. Sullivan, D. J. Salmon and T. J. Meyer, *Inorg. Chem.*, 1978, **17**, 3334.
18 (*a*) X.-C. Fu, M.-T. Li and C.-G. Wang, *Acta Crystallogr., Sect. E: Struct. Rep. Online*, 2005, **61**, m1221; (*b*) J. E. Fergusson and G. M. Harris, *J. Chem. Soc. A*, 1966, 1293; (*c*) F. Basolo and F. P. Dwyer, *J. Am. Chem. Soc.*, 1954, **76**, 1454.
19 (*a*) J. Casper and T. J. Meyer, *J. Phys. Chem.*, 1983, **87**, 952; (*b*) E. M. Kober, J. L. Masshall, W. J. Dressick, B. P. Sullivan, J. V. Casper and T. J. Meyer, *Inorg. Chem.*, 1985, **24**, 2755; (*c*) E. M. Kober, B. P. Sullivan, W. J. Dressick, J. V. Casper and T. J. Meyer, *J. Am. Chem. Soc.*, 1980, **102**, 7383; (*d*) J. V. Casper and T. J. Meyer, *J. Am. Chem. Soc.*, 1983, **105**, 5583; (*e*) J. V. Casper, E. M. Kober, B. P. Sullivan and T. J. Meyer, *J. Am. Chem. Soc.*, 1982, **104**, 630; (*f*) M. Bixon and J. Jortner, *J. Chem. Phys.*, 1968, **48**, 715; (*g*) K. F. Freed and J. Jortner, *J. Chem. Phys.*, 1970, **52**, 6272.
20 (*a*) S. E. Howson, L. E. N. Allan, N. P. Chmel, G. J. Clarkson, R. van Gorkum and P. Scott, *Chem. Commun.*, 2009, 1727–1729; (*b*) C. P. Sebli, S. E. Howson, G. J. Clarkson and P. Scott, *Dalton Trans.*, 2010, **39**, 4447–4454.
21 (*a*) *ShelXTL V.5*Siemens Analytical X-Ray Instruments, Inc.Madison, WI, U. S. A. 1994; (*b*) *ShelXL97*, G. M. Sheldrick, University of Göttingen, Germany, 1997.
22 M. J. Frisch, G. W. Trucks, H. B. Schlegel, G. E. Scuseria, M. A. Robb, J. R. Cheeseman, Jr., J. A. Montgomery, T. Vreven, K. N. Kudin, J. C. Burant, J. M. Millam, S. S. Iyengar, J. Tomasi, V. Barone, B. Mennucci, M. Cossi, G. Scalmani, N. Rega, G. A. Petersson, H. Nakatsuji, M. Hada, M. Ehara, K. Toyota, R. Fukuda, J. Hasegawa, M. Ishida, T. Nakajima, Y. Honda, O. Kitao, H. Nakai, M. Klene, X. Li, J. E. Knox, H. P. Hratchian, J. B. Cross, R. Ammi, C. Pomelli, J. W. Ochterski, P. Y. Ayala, K. Morokuma, G. A. Voth, P. Salvador, J. J. Dannenberg, V. G. Zakrzewski, S. Dapprich, A. D. Daniels, M. C. Strain, O. Farkas, D. K. Malick, A. D. Rabuck, K. Raghavachari, J. B. Foresman, J. V. Ortiz, Q. Cui, A. G. Baboul, S. Clifford, J. Cioslowski, B. B. Stefanov, G. Liu, A. Liashenko, P. Piskorz, I. Komaromi, R. L. Martin, D. J. Fox, T. Keith, M. A. Al-Laham , C. Y. Peng, A. Nanayakkara, M. Challacombe, P. M. W. Gill, B. Johnson, W. Chen, M. W. Wong, C. Gonzalez and J. A. Pople, *Gaussian 03, revision E.01*, Gaussian, Inc.: Wallingford, CT 06492, 2005.
23 (*a*) P. Hohenberg and W. Kohn, *Phys. Rev.*, 1964, **136**, B864; (*b*) W. Kohn and L. Sham, *Phys. Rev.*, 1965, **140**, A1133; (*c*) R. G. Parr and W. Yang, *Density Functional Theory of atoms and molecules*Oxford University Press: Oxford, U.K., 1989; (*d*) D. R. Salahub and M. C. Zerner, *The Challenge of d and f Electrons*, ACS, Washington, D.C., 1989.
24 (*a*) R. Bauernschmitt and R. Ahlrichs, *Chem. Phys. Lett.*, 1996, **256**, 454; (*b*) R. E. Stratmann, G. E. Scuseria and M. Frisch, *J. Chem. Phys.*, 1998, **109**, 8218; (*c*) M. E. Casida, C. Jamoroski, K. C. Casida and D. R. Salahub, *J. Chem. Phys.*, 1998, **108**, 4439.
25 (*a*) A. D. Becke, *J. Chem. Phys.*, 1993, **98**, 5648; (*b*) C. Lee, W. Yang and R. G. Parr, *Phys. Rev.*, 1988, **B 37**, 785; (*c*) B. Miehlich, A. Savin, H. Stoll and H. Preuss, *Chem. Phys. Lett.*, 1989, **157**, 200.
26 (*a*) P. J. Pulay, *J. Comput. Chem.*, 1982, **3**, 556.
27 H. B. Schlegel and J. J. McDouall, in *Computational Advances in Organic Chemistry*, Ed. C. Ogretir and I. G. Csizmadia, Kluwer Academic, The Netherlands, 1991, 167–185.
28 P. J. Hay and W. R. Wadt, *J. Chem. Phys.*, 1985, **82**, 270.
29 W. R. Wadt and P. J. Hay, *J. Chem. Phys.*, 1985, **82**, 284.
30 P. J. Hay and W. R. Wadt, *J. Chem. Phys.*, 1985, **82**, 299.
31 (*a*) W. J. Hehre, R. Ditchfield and J. A. Pople, *J. Chem. Phys.*, 1972, **56**, 2257; (*b*) P. C. Hariharan and J. A. Pople, *Theor. Chim. Acta*, 1973, **28**, 213; (*c*) P. C. Hariharan and J. A. Pople, *Mol. Phys.*, 1974, **27**, 209; (*d*) V. A. Rassolov, M. A. Ratner, J. A. Pople, P. C. Redfern and L. A. Curtiss, *J. Comput. Chem.*, 2001, **22**, 976; (*e*) M. M. Francl, W. J. Pietro, W. J. Hehre, J. S. Binkley, D. J. DeFrees, J. A. Pople and M. S. Gordon, *J. Chem. Phys.*, 1982, **77**, 3654.
32 (*a*) G. A. Petersson, A. Bennett, T. G. Tensfeldt, M. A. Al-Laham, W. A. Shirley and J. J. Mantzaris, *Chem. Phys.*, 1988, **89**, 2193; (*b*) G. A. Petersson and M. A. Al-Laham, *J. Chem. Phys.*, 1991, **94**, 6081.
33 (*a*) A. D. McLean and G. S. Chandler, *J. Chem. Phys.*, 1980, **72**, 5639; (*b*) R. Krishnan, J. S. Binkley, R. Seeger and J. A. Pople, *J. Chem. Phys.*, 1980, **72**, 650.
34 T. Clark, J. Chandrasekhar, G. W. Spitznagel and P. V. R. Schleyer, *J. Comput. Chem.*, 1983, **4**, 294.
35 N. M. O'Boyle, A. L. Tenderholt and K. M. Langner, *J. Comput. Chem.*, 2008, **29**, 839–845.
36 (*a*) M. Cossi, N. Rega, G. Scalmani and V. Barone, *J. Comput. Chem.*, 2003, **24**, 669; (*b*) V. Barone and M. Cossi, *J. Phys. Chem. A*, 1998, **102**, 1995.
37 (*a*) N. N. Greenwood, T. C. Gibb, *Mössbauer Spectroscopy*, Chapman and Hall: London, 1971; (*b*) G. M. Bancroft, *Mössbauer Spectroscopy: An Introduction for Inorganic Chemists and Geochemists*, McGraw-Hill: London, 1973.
38 (*a*) G. P. Souza, C. Konzen, J. D. Ardisson, H. A. D. Abreu, H. A. Duarte, A. F. C. Alcantara, W. C. Nunes, W. A. A. Macedo, M. Knobel and H. O. Stumpf, *J. Braz. Chem. Soc.*, 2006, **17**, 1534–1539; (*b*) D. Tudela and J. D. Tornero, *Inorg. Chim. Acta*, 1993, **214**, 197–199; (*c*) R. R. Berrett, B. W. Fitzsimmons and A. A. Osusu, *J. Chem. Soc. A*, 1968, 1575–1579; (*d*) G. M. Bancroft, M. J. Mays and B. E. Prater, *J. Chem. Soc. A*, 1970, 956–968.
39 (*a*) R. R. Berrett and B. W. Fitzsimmons, *Chem Comm.*, 1966, **91**; (*b*) R. R. Berrett and B. W. Fitzsimmons, *J. Chem. Soc. A*, 1967, 525–527.